We are IntechOpen, the world's leading publisher of Open Access books
Built by scientists, for scientists

4,800
Open access books available

122,000
International authors and editors

135M
Downloads

Our authors are among the

154
Countries delivered to

TOP 1%
most cited scientists

12.2%
Contributors from top 500 universities

CLARIVATE ANALYTICS
BOOK CITATION INDEX
INDEXED

WEB OF SCIENCE™

Selection of our books indexed in the Book Citation Index in Web of Science™ Core Collection (BKCI)

Interested in publishing with us?
Contact book.department@intechopen.com

Numbers displayed above are based on latest data collected.
For more information visit www.intechopen.com

Chapter

Analysis of Mechanical Properties of Austempered Ductile Iron Weld Joints Using Developed Electrode

Tapan Sarkar

Abstract

In the present investigation mechanical properties of austempered ductile iron (ADI) joints have been studied using two developed electrodes containing with and without Ce content and co-related between microstructure and mechanical properties. Austenitization was done at 900°C for 2 h and austempering at 300 and 350°C for 1.5, 2 and 2.5 h holding time. At 300°C microstructure shows needle shaped bainitic ferrite with lower amount of retained austenite indicate higher hardness and lower impact toughness. However, at 350°C shows feathery shaped bainitic ferrite with higher amount of retained austenite to demonstrate lower hardness and higher impact value. Both the welded joints at both austempering conditions tensile samples broke from the base metal indicates 100% joint efficiency. Fatigue life was varied with varying the austempering temperature and shows higher fatigue life at 350°C austempering temperature presence of higher amount of retained austenite and finer the bainitic ferrite size with smaller graphite nodules. Ce in weld metals to refine the microstructure and shows higher impact toughness and fatigue strength with lower hardness value at both austempering temperatures.

Keywords: heat treatment, microstructure, tensile test, Charpy impact, high cycle fatigue

1. Introduction

Austempered ductile iron (ADI) is a new family member of engineering materials. It has recently received significant attention owing to the excellent combination of mechanical properties such as high strength together with good ductility, good wear resistance, and higher fatigue strength to make the material as a successful substitute for forge steels or aluminum alloys [1–4]. The remarkable properties of the ADI are attributed with the unique microstructural constituents such as bainitic ferrite and high carbon enriched retained austenite.

The low production cost and production advantage of ADI, it has been used in many structural applications and many critical parts of automobiles such as crankshaft, steering knuckles, hypoid rear axle gears, camshafts and disk-brake calipers etc. in which fatigue resistance is an important requirement [5, 6].

ADI shows higher fatigue life than as-cast ductile iron (DI) and determined by generating stress-life (S-N) curves [7]. The fatigue life of ADI strongly depends on the austempering temperature, austempering holding time, austempering kinetics,

the amount of retained austenite, shape and size of bainitic ferrite and graphite nodules [1, 3].

The chemical composition of ADI is similar to conventional DI. However, some alloying elements such as Ni, Cu and Mo are usually added to increase the austemperability, to delay the austenite decomposition [8, 9] to pearlite and ferrite upon cooling. DI converts to ADI with the help of two steps isothermal heat treatment process. Austenitization was done at 850–910°C for 30 min–2 h holding time and austempering at 250–450°C for 5 min–4 h holding time and finally cooled at room temperature in the open air [10]. The total heat treatment process depends on the chemical composition and thickness of the as-cast DI. Austempering temperature and holding time shows significant effects on the microstructure and mechanical properties of ADI. During austempering two-stage reactions have been done, at the initial stage (stage I) austenite (residual austenite) decomposed into bainitic ferrite and high carbon austenite (retained austenite). Increasing holding time the stage II reaction was start and high carbon austenite further decomposed into bainitic ferrite and carbide (ε carbide). The time periods between the two stage reactions is called the process windows, obtained optimum combination of microstructural and mechanical properties. Presence of alloying elements such as Ni, Cu and Mn to delay the austempering reaction and increased the process windows [11].

At a lower austempering temperature ADI shows needle shaped bainitic ferrite with a lower amount of retained austenite and graphite nodules, which in turns increased the tensile strength and hardness to decrease the elongation and toughness. However, at higher austempering temperature shows coarser bainitic ferrite with higher amount of retained austenite and graphite nodules, as a result to decrease the tensile strength and hardness; increased toughness that illustrate higher fatigue strength [6, 10, 12].

It is reported, the fatigue strength of ADI is not only depended on tensile strength and hardness like as steel [13]. However, in ADI the amount of retained austenite and its carbon content, size of graphite nodules, nodularity, shape and size of bainitic ferrite plays an important role in the high cycle fatigue performance and higher fatigue limit [1, 13–15]. Bahmani et al. [16] illustrate a relationship between the microstructure and fatigue strength of ADI and obtained, the fatigue strength depended on the amount of retained austenite and its carbon content. The fatigue strength was increased as increasing the amount of retained austenite and its carbon content. Graphite nodularity and its size show significant effects in fatigue life. In ADI graphite working as a shrinkage cavities. During fatigue test, micro crack was initiated around the graphite and then formed to macro crack which leads to the final failure of the sample [17]. Sofue et al. [18] reported, with increasing the graphite size to decrease the fatigue strength and the fatigue strength was optimized by decreasing the graphite nodule size.

Further, rare earth metal such as cerium has a beneficial effect on the microstructure and properties of ADI. However, the optimum rare earth content varies significantly according to different investigators. For example, researchers [19] reported that the presence of Ce content from 0.005 to 0.014% the nodularity was increased with refining the size of the nodules but further increasing Ce content up to 0.018 or 0.020%, the nodularity decreased and formed some non-spherical graphite with coarsening the nodule size to decreased the fatigue strength. Choi et al. [20] observed that DI castings with 0.3% rare earth content attributed improved graphite nodules, lower tensile strength and hardness, higher elongation to indicate the higher fatigue strength than that of DI castings without rare earth.

However, in spite of high strength, reasonable ductility and higher fatigue life, the application of ADI is somehow limited due to non-availability of a suitable electrode which has inhibited the joining of such high potential material.

Furthermore, many a time ductile iron castings for converting ADI need to repair welding which also demands welding consumables compatible with DI base materials. Commercially available coated electrodes for welding conventional DI include pure nickel (90–97%) [21], stainless steel and iron-nickel [22] which are first of all not suitable for converting ADI from DI weld due to poor austemperability and also not cost-effective [21, 22]. Recent authors successfully developed a coated electrode for welding DI [23] and convert to ADI after heat treatment, obtained higher tensile strength and toughness. Further improvement of the weldability of DI and welding of higher grade DI to obtain higher toughness and fatigue strength, coated electrode was developed to introduce nano-CeO_2 as a flux ingredient [24].

However, all the previous literature discussed about the fatigue strength or fatigue life only on DI or ADI base metal [1, 14, 25, 26]. But there is no such a literature to discuss about the fatigue life of ADI weld joints. Owing to the importance of the ADI especially on structural and automobile application, it is needed to find out the fatigue properties of ADI weld metal to use in commercial application.

The present work thus aims is to study the mechanical properties of ADI weld joints and co-relation between as-cast and heat treated microstructure, using two developed electrodes. Microstructural studies were done using optical microscopy (OM) and scanning electron microscopy (SEM). Phase analysis was performed utilizing XRD analysis and mechanical properties of the weld joints performed under microhardness, transverse tensile, room temperature Charpy impact and high cycle fatigue (HCF) test. Fatigue crack growth and fatigue fracture surface were investigated under SEM studies.

2. Experimental procedure

As cast DI was collected from the local foundry and used as a base metal for this experimental purpose. The details chemical composition of the as-cast DI is given in **Table 1**.

Two developed electrodes containing without and with Ce such as Trial 4 and Trial 7 selected for the experimental purpose. Among the two electrodes, Trial 4 contents with without Ce and Trial 7 contents with Ce content (0.1%). The details chemical composition of the two developed electrodes is given in **Table 2**.

Modified U groove (**Figure 1**) weld was performed on the DI base plate using both Trial 4 and Trial 7 electrodes applied shielded metal arc welding (SMAW) process. Preheat was applied at 300°C for 1 h and post weld heat treatment (PWHT) at 300°C for 1 h immediate after welding using the constant welding parameters [27, 28]. The details welding parameters are given in **Table 3** and the defect free weld was considered as per AWS (D11) [29].

The welded DI specimens are converted to ADI with the help of two steps isothermal heat treatment process. Austenitization was done at 900°C for 2 h holding time and then samples are immediately transferred to salt bath for austempering process. Austempering was done at 300 and 350°C for 1.5, 2 and 2.5 h holding time than air cooled to room temperature. Typical isothermal heat treatment cycle is shown in **Figure 2**.

Element	C	Si	Mn	S	Cr	Mg	P	Fe
Wt.%	3.60	2.92	0.22	0.019	0.028	0.041	0.01	93.16

Table 1.
Chemical composition of as-cast ductile iron.

Element wt.%	C	Mn	Si	S	P	Ni	Mo	Cu	Al	Bi	Mg	Ca	Ti	Fe	Ce
Trial 4 (without Ce)	3.08	0.40	2.60	0.006	0.039	0.5	0.19	0.24	0.62	0.03	0.004	0.015	0.09	91.40	—
Trial 7 (with Ce)	3.28	0.43	2.76	0.008	0.02	0.66	0.31	0.29	0.48	0.03	0.003	0.003	0.14	91.45	0.10

Table 2.
Chemical composition of the weld deposits using developed coated.

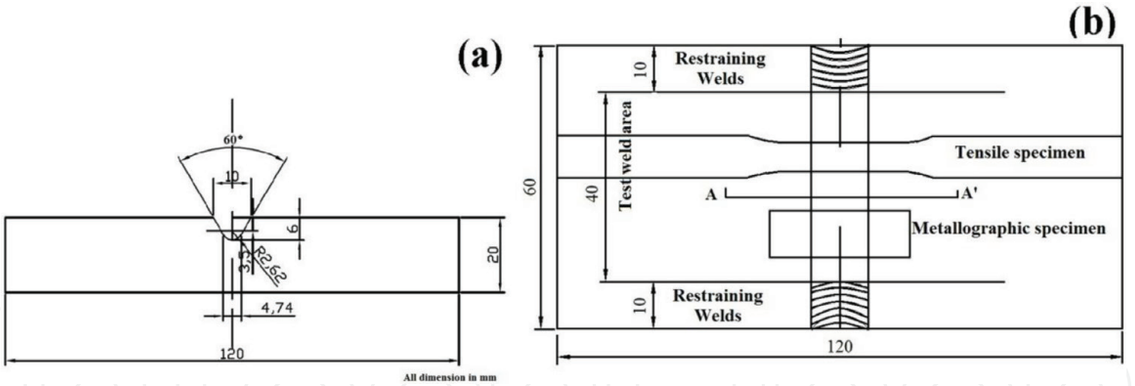

Figure 1.
(a) Modified grove design, (b) schematic view of extracting samples from weld metal.

Parameters	Unit	Value
Preheat temperature (1 h)	°C	300
PWHT (1 h)	°C	300
Welding current	A	150
Arc voltage	V	24
Welding speed	mm/s	1.70
Heat input	kJ/mm	1.58

Table 3.
Defect free weld procedure.

Metallography samples of 20 × 10 × 15 mm dimensions were cut from the large size weld specimen and removed any decarburized skin by surface grinding. Samples were mounted at room temperature, then polished systematically in silicon carbide paper and followed by cloth polishing using 0.5 μm alumina solution. Polished samples were etched with 5% nital solution and microstructures are studied under an optical microscopy (Carl Zeiss made: AXIO Imager A1m) and photographs are taken at 500× magnification. For better clarity, samples were studied under scanning electron microscopy (SEM) (JEOL JSM-5510 with INKA software EDS system using an ultra-thin window detector) and photographs were taken at higher magnifications.

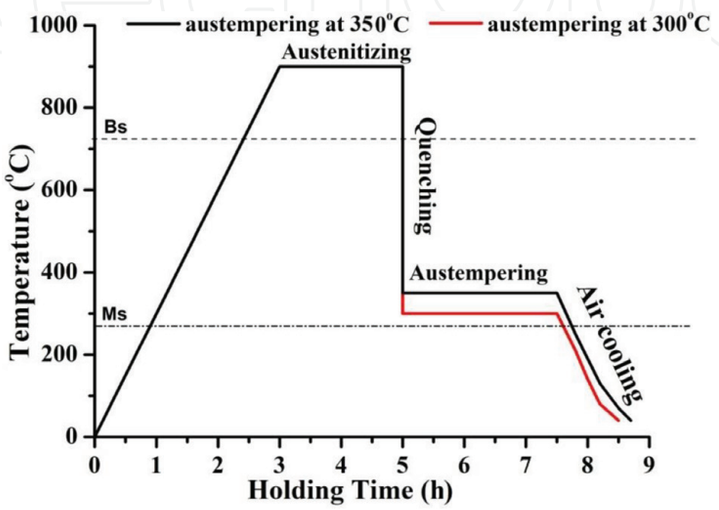

Figure 2.
Typical heat treatment cycle.

X-ray diffraction (XRD) analysis was performed to estimate the volume fraction of retained austenite and its carbon content using anode Co-K_α radiation in 1.79026 targets with 24 kV and tube current was 40 mA. The specified 2θ range was varied from 30 to 110° with a step size of 0.2°/min. Detailed XRD analysis was performed using integrated intensities of the positions and the integrated intensities for the {1 1 1}, {2 2 0} and {3 1 1} planes of FCC austenite as well as the {1 1 0} and {2 1 1} planes of BCC ferrite. The volume fraction of retained austenite was calculated using the following empirical formula [30]:

$$X_\gamma = \frac{I_\gamma / R_\gamma}{(I_\gamma / R\gamma) + (I_\alpha / R_\alpha)} \quad (1)$$

Where I_γ and I_α are the integrated intensities and R_γ and R_α are the theoretical relative intensity for the austenite and ferrite, respectively, and Bainitic ferrite was calculated by using the formula:

$$X_\gamma + X_\alpha + X_g = 1 \quad (2)$$

Where, X_γ and X_α and X_g represent the volume percentage of retained austenite, volume percentage of bainitic ferrite and volume percentage of graphite. The carbon concentration of the austenite was determined using the equation [30].

$$a_\gamma = 0.3548 + 0.0044\, C_\gamma \quad (3)$$

Where a_γ is the lattice parameter of austenite (in nm) and C_γ is the carbon content of austenite (in wt.%). The {1 1 1}, {2 2 0} and {3 1 1} planes of austenite were used to estimate the lattice parameter.

Vickers microhardness test of the weld metals was performed at room temperature using Leco Vickers microhardness tester (Model LM 248SAT) with 100 gf load at 10 s holding. The hardness values were taken from six different positions of each weld specimens and the average of the six values considered the final one.

Tensile properties such as ultimate tensile strength (UTS), yield strength (YS) and % elongation of the welded joints were evaluated using transverse tensile specimen keeping the weld metal at the center of the gauge length. The tests were performed under uniaxial loading at a crosshead speed of 5 mm/min in universal tensile testing m/c (Instron 8862).

Sub-size (55 × 10 × 3.3 mm) and without notch transverse Charpy impact test of the ADI welded joints were performed at room temperature according to ASTM E-23 [31]. Four samples were tested at each austempering condition (300 and 350°C for the 2 h holding time) and an average of four values has been reported.

High cycle fatigue (HCF) test of transverse weld samples as per ASTM E466-15 [32] (**Figure 3**) were performed using Rumul resonant testing machine to determine

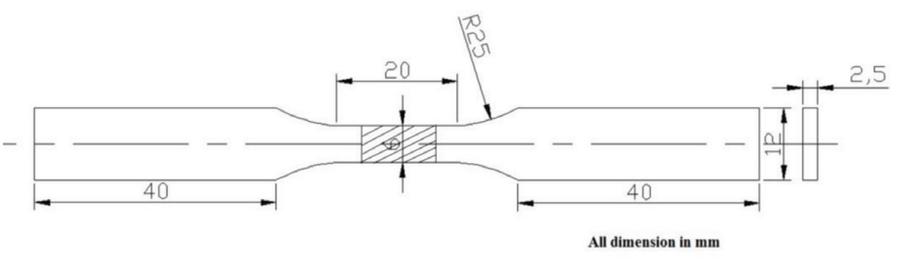

Figure 3.
Schematic view of transverse high cycle fatigue sample as per ASTM 606.

the S-N curve. The tests were run to failure up to 10^7 cycles at constant stress control mode and the number of cycles of failure was recorded with keeping the load ration R at 0.1. The stress levels were varied between 30 and 80% of Yield strength to obtaining the endurance limit and S-N curve was plotted by stress amplitude and the number of cycles in log-log scale.

After successfully testing, fracture surface and crack path of the tested samples were studied under SEM and fractographs were taken at different magnifications.

3. Results and discussion

3.1 Microstructure

3.1.1 Base metal

Figure 4 shows the optical microstructure of as-cast DI (base metal). The microstructure shows graphite nodules surrounded with ferrite matrix. The average nodularity shows 90% with 130 nodules per unit area (mm^2) and average nodule size is r = 18.5 μm.

3.1.2 As-welded microstructure

The optical microstructures of weld metals using two selected coated electrodes containing without and with Ce is shown in **Figure 5**. In **Figure 5a** and **b**, the microstructure shows ledeburitic carbide (LC), alloyed pearlite (AP) and graphite nodules (G). In both the weld metal microstructure shows small amount of graphite nodules with smaller in size due to higher cooling rate experienced in weld metal. Although both the as-weld microstructure shows similar microstructural appearance, a close look into the microstructure reveals difference in grain size and volume percentage of ledeburitic carbide and alloyed pearlite. The presence of Ce in weld metal has caused the structure finer (the finer the dendritic structure), lesser ledeburitic carbide, higher amount of alloyed pearlite and increasing the graphite volume percentage and nodularity.

It has been shown that cerium reduces both primary [33] and secondary [34] dendritic arm spacing as well as inhibit the development of columnar crystal.

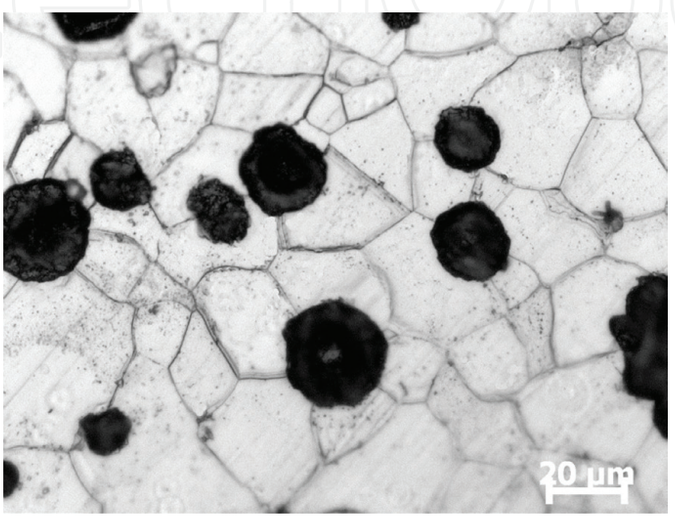

Figure 4.
Optical microstructure of as-cast ductile iron.

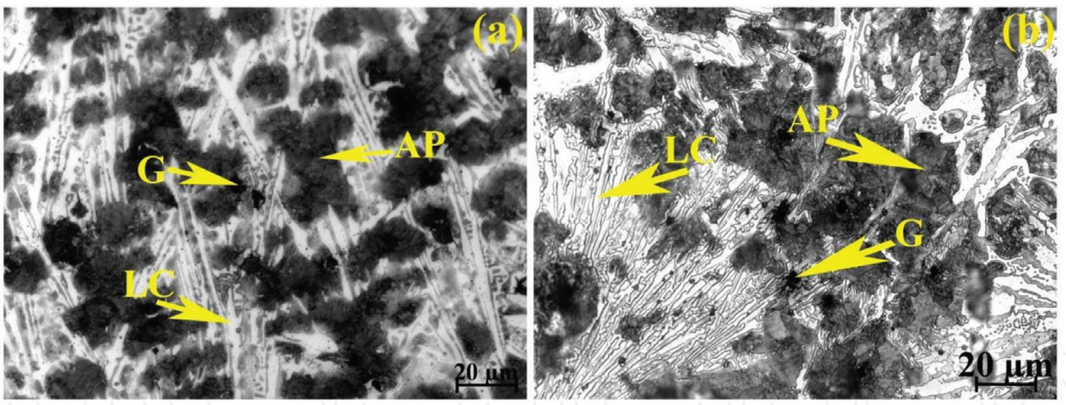

Figure 5.
Optical microstructure of as-welded weld metal (a) Trial 4 (b) Trial 7.

Also, the degree of supercooling for rare earth treated steel has been reported to be smaller than rare earth free steel [35]. The refined microstructure (**Figure 5b**) that has been observed for Ce treated weld metal is presumably due to the fine primary austenite dendrite and suppression of columnar grain growth during solidification of the weld pool. Furthermore, it is believed that smaller degree of super cooling associated with Ce treated weld metal has caused reduction in ledeburitic carbide.

Ce acts as a modifying element on DI as a form of deoxidization and desulfuration [36]. Ce reacts with oxygen and sulfur to form Ce-rich oxides, Ce-rich sulfides or Ce-rich oxide-sulfides formed in DI welds and act as a heterogeneous nuclei of primary carbides, according to the principle of crystallography so that the nuclei of primary carbides can form and grow everywhere in molten metal [37] and refine the structure. Furthermore, cerium content present in the carbide as a form of Ce_2S_3 and CeO_2 (measured by X-RD analysis) and increase the solidification rate to refine the structure [37].

3.1.3 Austempered microstructure

After austempering heat treatment the weld metal microstructure consists of bainitic ferrite (BF) and retained austenite (RA) matrix with graphite nodules (G). **Figure 6a** and **b** illustrate the weld metal microstructure after austempering at 300 and 350°C for 2 h holding time using Trial 4 electrode. Similarly, **Figure 6c** and **d** illustrate weld metal structure after austempering at 300 and 350°C for 2 h holding time using Trial 7 electrode. In both the weld metals austempering at 300°C, the microstructure (**Figure 6a** and **c**) shows needle shape bainitic ferrite, retained austenite and graphite nodules. Whereas at 350°C (**Figure 6b** and **d**) shows feathery shape (lath type) bainitic ferrite with retained austenite and graphite nodules.

For better clarity, the microstructures of heat treated weld metals after austempering at 300 and 350°C for 2 h holding time were studied under SEM and the structures are shown in **Figure 7** for without and with Ce containing weld metals respectively.

Interestingly, both the weld metal shows the same microstructural appearance at respective austempering conditions. But the structures were varied in morphology, amount, shape and size of bainitic ferrite, amount of retained austenite, nodule size and nodularity with changing the austempering conditions and type of electrode used (without and with Ce containing).

However, at 350°C more amount of retained austenite and lesser amount of bainitic ferrite was observed; but the opposite trend in microstructural constituents has been revealed at 300°C i.e. lower amount of retained austenite and higher amount bainitic ferrite. The nodularity also varied with varying the austempering temperatures and higher nodularity is observed at 350°C at both the weld metals. The microstructural constituents also changed with changing the austempering

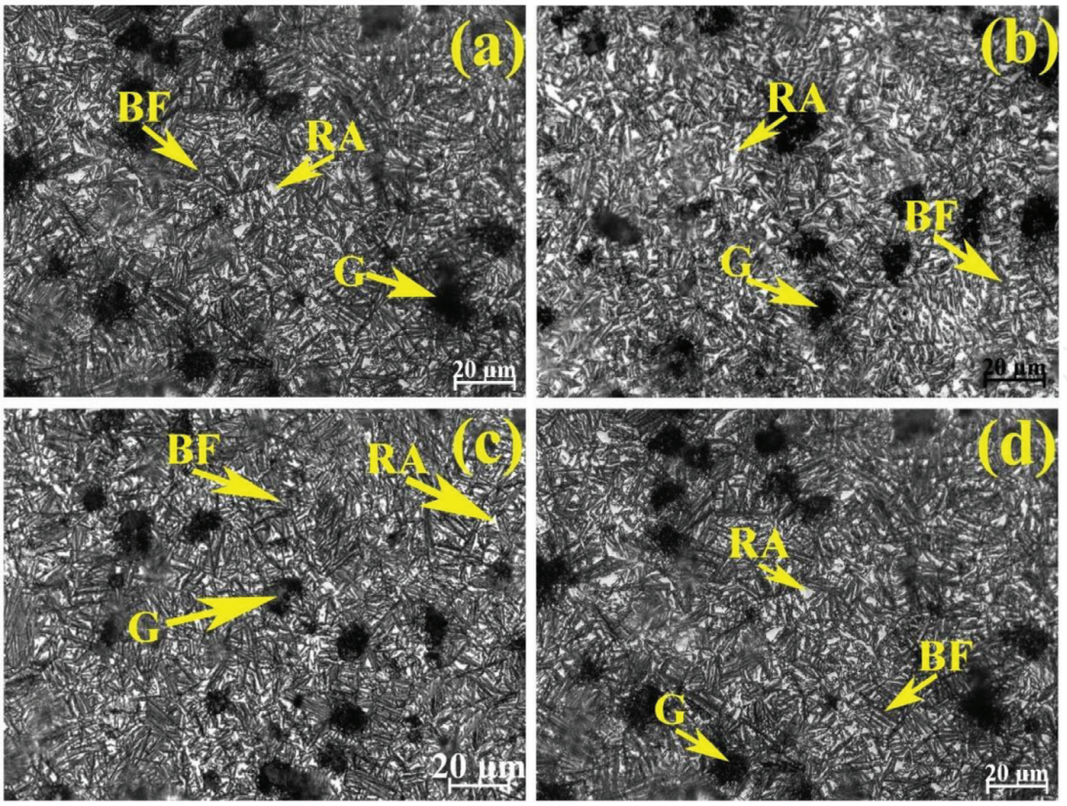

Figure 6.
Optical microstructure of weld metal austempered at (a) 300°C (b) 350°C for 2 h holding time using Trial 4 and (c) 300°C (d) 350°C for 2 h holding time using Trial 7 coated electrode.

holding time at a given temperature [9]. However, for both the austempering temperatures the variation of the microstructural constituent is similar i.e. with changing the holding time from 1.5 to 2 h the amount of retained austenite was increased and the amount of bainitic ferrite was decreased also refine the bainitic

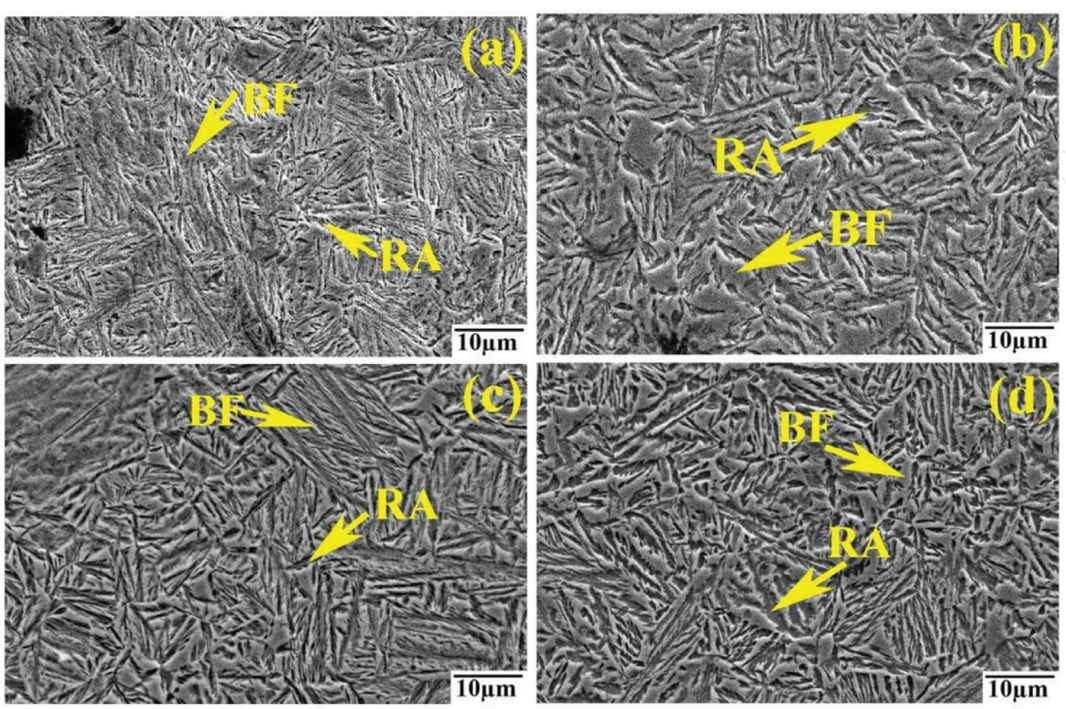

Figure 7.
SEM microstructure of weld metal austempered at (a) 300°C (b) 350°C for 2 h holding time using Trial 4 and (c) 300°C (d) 350°C for 2 h holding time using Trial 7 coated electrodes.

ferrite shape and size. Further increasing the austempering holding time from 2 to 2.5 h the amount of retained austenite was decreased and the amount of bainitic ferrite was increased. Interestingly, at both 300 and 350°C austempering temperature for 2 h holding time the carbon enrichment in austenite is maximum (**Figure 9**) which has caused to stabilize more amount of retained austenite (**Figure 8**) at both the austempering conditions after cooling to room temperature. However, at higher holding time (2.5 h) untransformed austenite transformed to carbides (ε carbide) and bainitic ferrite leading to decrease the amount of retained austenite content [1].

The observed finer and homogeneous structure along with increasing the amount of retained austenite (**Figure 8**) with the presence of Ce content in weld metal. At both 300 and 350°C austempering temperature microstructure attributed finer the bainitic ferrite size, higher amount of carbon enriched retained austenite and higher graphite nodularity was observed with presence of Ce in weld metal. The carbon enrichment of austenite will be faster in Ce treated weld metal due to lesser diffusion distance for carbon, which diffuses from fine cementite lamellae of pearlite. Also, smaller the nodule size having more surface area to volume ratio will favor carbon diffusion from graphite [38]. Thus, with the increase of carbon content of initial austenite the driving force of stage I reaction become slow and delay the transformation rate of bainitic ferrite due to drag effects of Ce. As a result more amount of carbon was diffused to the surrounding austenite and austenite become more stable.

3.1.4 Volume percentage of retained austenite and its carbon content

The volume percentage of retained austenite and its carbon content of both the weld metals after austempering at 300 and 350°C for different holding times have been calculated from X-RD analysis. The variation of retained austenite with changing the holding time (1.5, 2 and 2.5 h) at 300 and 350°C austempering temperature has been plotted in **Figure 8**. In **Figure 8**, it is seen that at both 300 and 350°C temperature both the weld metal (without and with Ce containing) the amount of retained austenite was changed with changing the austempering holding time. Holding time changed from 1.5 to 2 h the amount of retained austenite was increased with decreasing the amount of bainitic ferrite. With further increases the holding time from 2 to 2.5 h the amount of retained austenite was decreased. Although the nature of change the amount of retained austenite is same at both

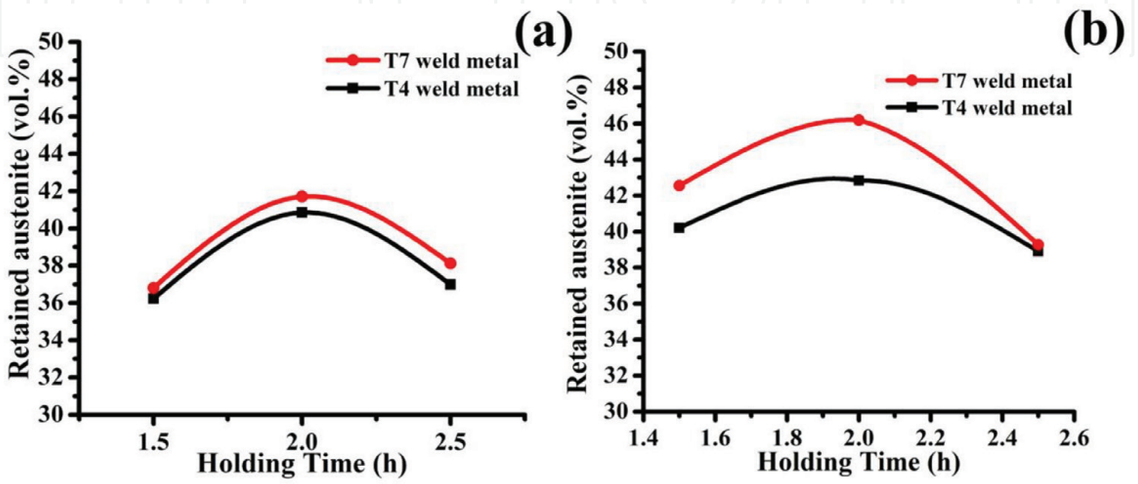

Figure 8.
Volume percentage of retained austenite content at different holding time of weld metal austempering at (a) 300°C and (b) 350°C using Trial 4 and Trial 7 electrodes.

the austempering temperature of both the weld metals, austempering at 350°C shows the higher amount of retained austenite compared to 300°C at each holding time. This could be due to the higher diffusion rate of carbon during bainitic ferrite transformation at higher austempering temperature [39].

Bainitic ferrite formation is a growth process; during austempering process bainitic ferrite is transformed from the existing austenite (residual austenite). During the transformation of bainitic ferrite, carbon was diffused from the bainitic ferrite to the surrounding austenite to make the austenite stable, and this austenite is called untransformed austenite or retained austenite. At lower austempering temperature, due to higher super cooling the transformation rate of bainitic ferrite is high and diffused less amount of carbon to the surrounding austenite, as a result formed less amount of retained austenite in weld metals. Furthermore, at higher austempering temperatures, due to lower supper cooling the growth of bainitic ferrite is high and diffused higher amount of carbon content to the surrounding austenite and shows higher amount of retained austenite in weld metals.

Ce is a modifying alloying element and act as a nodularizing and austempering element during austempering process. The presence of Ce in weld metal to slow the austempering kinetics and prolongs to the stage I reaction. As a result higher amount of carbon was diffused during the transformation of bainitic ferrite to the surrounding austenite and show a higher amount of retained austenite at both the austempering temperature than without Ce content weld metal also refine the microstructure to indicate higher toughness and longer fatigue life.

Furthermore, the carbon content of retained austenite in two weld metals (without and with Ce containing) at 300 and 350°C for 1.5, 2 and 2.5 h holding time have been determined using the empirical formula (2). The calculated results of the amount of carbon present in austenite at 300 and 350°C for different holding times have been plotted in **Figure 9**. In **Figure 9**, it is seen that, in both the weld metals, the trend in variation of carbon content in retained austenite with changing the austempering holding at 300 and 350°C is similar to the variation of retained austenite (**Figure 8**). The maximum amount of carbon content was achieved at 2 h holding time irrespective of the austempering temperature and electrode composition. Weld metal containing Ce show the highest carbon content (2.2 wt.%) in retained austenite at 350°C for 2 h holding time.

During austempering transformation, bainitic ferrites are nucleated out of austenite (residual austenite) to refusing the carbon content to the surrounding austenite

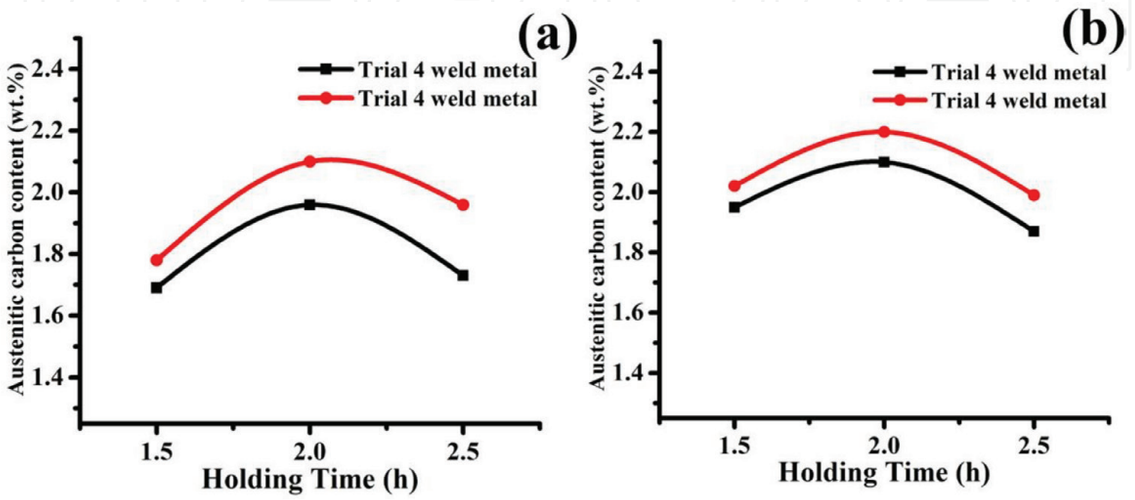

Figure 9.
Austenitic carbon content of weld metal at different holding time austempering at (a) 300°C and (b) 350°C using Trial 4 and Trial 7 electrodes.

and austenite become stabilized. Thus, maximum stability of retained austenite should possess at 2 h holding time, irrespective of austempering temperature of both the weld metals.

3.2 Mechanical properties

The mechanical properties of ADI welded joints depends on the amount of retained austenite and its carbon content presence in microstructure [1, 2, 40]. Mechanical properties were varied with varying the austempering temperature and it's holding time due to the variation of microstructural constitutes, shape and size, nodularity and numbers of nodule presence in per mm^2. At 300°C austempering temperature microstructure consists of needle shaped bainitic ferrite with small amount of retained austenite indicates higher tensile strength and hardness with lower the toughness. However, at 350°C austempering temperature structure shows feathery shaped bainitic ferrite with higher amount of retained austenite indicated lower tensile strength and hardness with higher toughness and fatigue strength. The average mechanical properties of both the weld metals (Trial 4 and Trial 7) after austempering at 300 and 350°C for 2 h holding time are given in **Table 4**.

3.2.1 Microhardness

The microhardness of both the weld metals (without and with Ce containing) after austempering at 300 and 350°C for 1.5, 2 and 2.5 h holding time were taken at six different positions of the weld metal and the average of six considered final value. The average microhardness of the weld metals at both 300 and 350°C austempering temperature are plotted in **Figure 10** with respect to the holding time. **Figure 10** demonstrates that at 300°C both the weld metal shows higher hardness value than 350°C due to the variation of the amount of carbon enriched austenite. However, the hardness values are changed with changing the austempering holding time. In both the weld metals at both 300 and 350°C holding time changed from 1.5 to 2 h, the hardness values are decreased with increasing the amount of retained austenite. With increasing holding time from 2 to 2.5 h the hardness values are increased, with decreasing the amount of carbon enriched retained austenite in weld metals. At higher holding time the stage II reaction was started and the carbon enriched retained was diffused to bainitic ferrite and carbide, as a results the amount of retained austenite was decreased and the hardness value increased [41]. At both the austempering temperature of both weld metals at 2 h holding time attributed lower hardness value, the presence of higher amount of retained austenite.

Further, at each austempering conditions Ce containing weld metal shows lower hardness value due to higher amount of carbon enriched retained austenite in weld

Electrode	Austempering temperature (°C)	Holding time (h)	Charpy impact (J)	Fatigue strength (MPa)	Microhardness (Hv)
Trial 4 (without Ce)	300	2	20	211	327
	350		26	241	280
Trial 7 (with Ce)	300		22	241	290
	350		31	302	273

Table 4.
Mechanical properties of ADI weld metals.

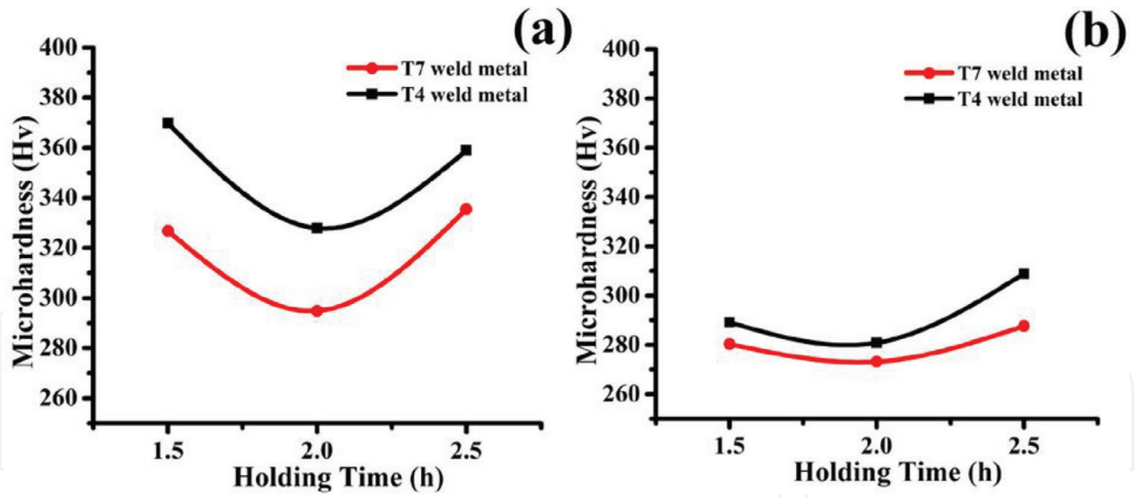

Figure 10.
Variation of microhardness of weld metals at different holding time austempering at (a) 300°C and (b) 350°C using Trial 4 and Trial 7 electrodes.

metal and attributed minimum hardness (273Hv) at 350°C for 2 h holding time presence of higher amount of retained austenite (46.7%) compared to without Ce content weld metal.

3.2.2 Tensile test

The transverse tensile tests of Trial 4 and Trial 7 weld joints after austempering at 300 and 350°C for 2 h holding time were carried out. For both the austempering conditions of both the weld metals failure of the test samples took place from the base metal as shown in **Figure 11**, indicating that weld metal is stronger than base metal. Thus the transverse tensile results show 100% joint efficiency of ADI weld metals (at 300 and 350°C for 2 h holding time) indicating successfully development of coated electrode and establishment of a weld procedure which could be applied commercially.

The tensile properties of ADI is strongly depends on the amount of retained austenite and its carbon content, the shape and size of bainitic ferrite and the numbers of graphite nodules presence in per unit area [42, 43]. At each austempering conditions both the weld metal attributed more amount of retained austenite and finer bainitic ferrite and smaller size of graphite nodules compare to base metal and HAZ. During tensile testing weld metal is possibly more strain hardened compare to base metal and HAZ due to presence of higher amount of retained austenite [43, 44]. It is well known that austenite having FCC structure possesses higher strain hardening rate than BCC ferrite (bainitic ferrite) and the strain hardening rate of austenite also increases with presence of carbon content [45]. Thus, one would expect, due to more amount of retained austenite along with higher carbon, that tensile strength of Ce containing weld metal would be higher than weld metal having without Ce at 350°C austempering temperature for 2 h holding time.

3.2.3 Charpy impact test

The average sub-size Charpy impact values of without and with Ce containing weld metals after austempering at 300 and 350°C for 2 h holding time are given in **Table 4**. The result states that the Charpy impact values are increased with increasing the austempering temperature from 300 to 350°C. The Charpy impact values are strongly depends on the amount of retained austenite, shape and size of bainitic

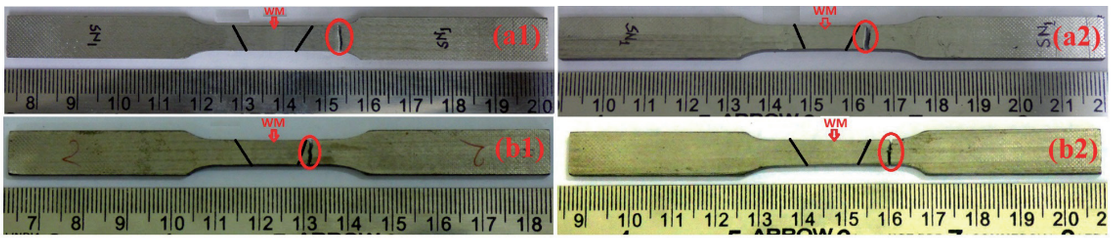

Figure 11.
Transverse tensile samples after testing, austempering at (a1) 300°C, (a2) 350°C for 2 h using Trial 4 and (b1) 300°C, (b2) 350°C for 2 h using trial electrode.

ferrite, graphite nodularity, size of the nodules and numbers of nodules presence in per unit area. Presence of higher carbon content in austenite the strain hardening rate of austenite is high and consequently more energy is being absorbed leading to increase in impact toughness [42, 43]. The higher nodularity could suppress the crack initiation due to lower stress concentration and increase in amount of graphite nodules could act as crack arrester during impact testing. Therefore, increasing the graphite nodularity of ADI can improved the high cycle fatigue strength. In both the weld metals at 350°C to attributed higher carbon enriched retained austenite to signify the higher impact values.

Furthermore Ce containing weld metal shows higher Charpy impact values at both the austempering temperature. Ce content in weld metal to refine the bainitic ferrite and retained austenite shape with increased the amount of retained austenite content, smaller the graphite nodules with higher nodularity indicates higher impact values. The highest impact value (31 J) was obtained at 350°C at Ce content weld metal presence of maximum amount (46%) of carbon enriched retained austenite.

The fracture surfaces of the freshly broken Charpy impact test specimens of both Trial 4 and Trial 7 after austempering at 300 and 350°C for 2 h holding time were examined under SEM in order to relate impact properties to operative fracture mechanism and are given in **Figure 12**. At 300°C both the weld metal (**Figure 12a** and **c**) fracture surface exhibits predominantly dimple and quasi-cleavage types fracture. However, at 350°C (**Figure 12b** and **d**) the fracture surface exhibits predominantly

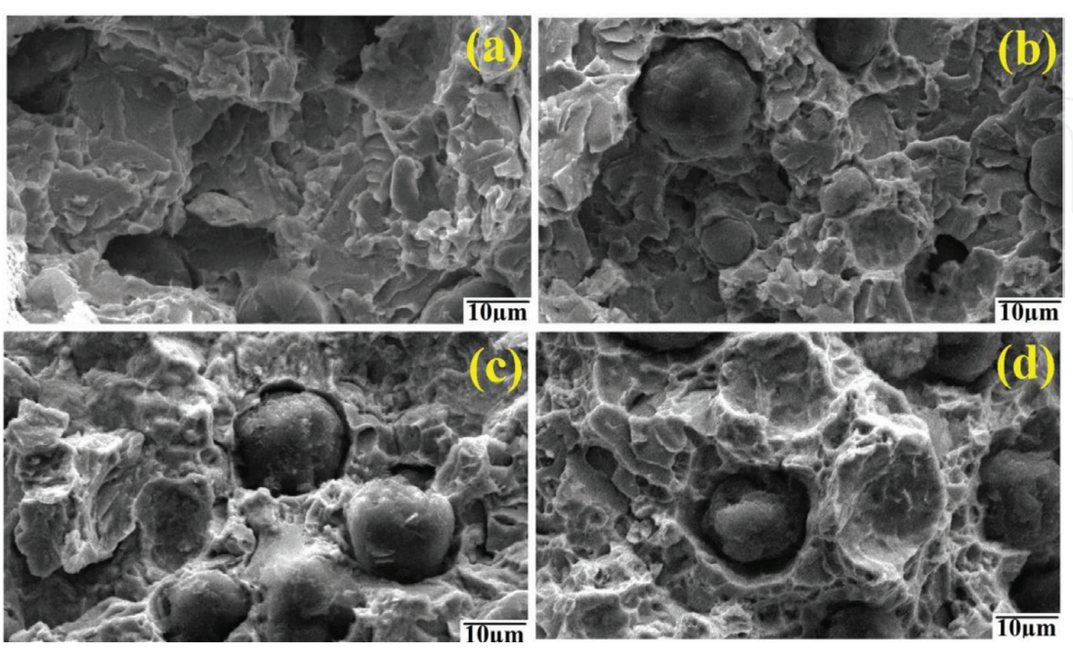

Figure 12.
Fracture surface of ADI weld metal austempering at (a) 300°C and (b) 350°C for 2 h using Trial 4 and (c) 300°C and (d) 350°C for 2 h using Trial 7 developed electrode.

dimple in nature ductile fracture of both the weld metals. The presence of Ce content in weld metal the sizes of the dimple are more fine and with changing the austempering temperature (300–350°C) the shape and size of dimple are more finer to indicate the higher impact value. It appears that extensive plastic flow around the graphite nodules results in stress concentration at graphite-matrix interface which leads to a decohesion between graphite nodules and the matrix. **Figure 12** illustrates the small graphite nodules within cavities or dimples that initiated the microvoids. Subsequent growth and coalescence of these microvoids produced dimple rupture network. The crack, which is likely to initiate near the graphite nodule, propagates through the matrix to reach the adjoining nodules. It is anticipated that plastic deformation in the matrix ahead of the regions of decohesion will thus be confined essentially to the soft ferrite regions [42] and the crack propagation becomes difficult across the tough austenite to join up with similar micro cracks in the neighboring ferrite needles. Therefore, one can expect improved toughness with increasing the volume fraction of retained austenite.

3.2.4 High cycle fatigue analysis

The fatigue life of weld joints after austempering at 300 and 350°C using without and with Ce containing coated electrodes are represented through S-N curve in **Figure 13**. The S-N curve is drawn through the data point as best fit line and the arrows are indicates the samples did not fail before an excess of 10^7 cycle or more stress cycle to called the endurance limit. The maximum strength obtained at 10^7 cycles is called the fatigue strength. In **Figure 13** illustrate that the fatigue strength of the weld joints were varied with varying the austempering temperature and respective weld metal composition. The maximum fatigue strength (302 MPa) was obtained at 350°C for with Ce weld metals due to higher toughness and lower tensile strength and hardness of weld metal (**Table 4**).

At lower (300°C) austempering temperature microstructure shows needle shape bainitic ferrite with lower amount of retained austenite to indicate higher tensile strength and hardness with lower impact toughness. However, at higher (350°C) austempering temperature microstructure shows coarser bainitic ferrite with higher amount of retained austenite to indicates lower tensile value and hardness with higher impact toughness indicates higher fatigue strength.

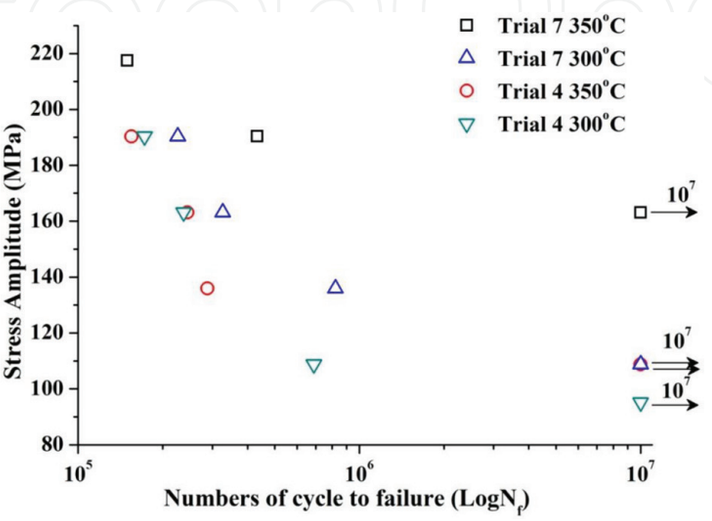

Figure 13.
Comparison of S-N curve of high cycle fatigue test for Trial 4 and Trial 7 weld metals at different austempering conditions (arrow indicating the endurance limit of the each condition).

The fatigue strength of ADI joints depended on the amount of retained austenite and its carbon content presence in ADI weld metals and the values are increased with increasing the amount of retained austenite content due to the higher strain hardening behavior of austenite [46]. Owing to the higher strain hardening behavior of austenite to delay the formation of persistent slip bands and reduces the nucleating of fatigue crack growth. However higher amount of retained austenite transformed to plastic induced martensite during high cycle fatigue test [26, 46, 47]. Such types of transformation was occurred at the plastic zones to ahead the fatigue crack and relax the stress concentration at the crack tip, as a result to reduce the fatigue crack growth rate and increase the fracture toughness.

However, the fatigue strength also depends on the shape and size of the bainitic ferrite, retained austenite and graphite nodules. The fatigue strength of ADI was improved when the nodule count was increased, in particular at austempered temperatures for higher toughness [26]. Therefore, ADI with a higher nodule count with the smaller size exhibits a better fatigue life [26]. The more pronounced graphite nodule size with higher optimum toughness to exhibits higher amount of retained austenite indicates maximum fatigue strength.

Presence of Ce content in weld metal illustrates higher fatigue strength than without Ce content weld metal. Ce content to refine the austenitic grain size also increasing the amount of retained austenite and its carbon content to illustrate the higher fatigue life. The smaller retained austenite grain size apparently creates more dislocation barrier; as a result the formation of precipitate slip band is more difficult and required more number of cycles to initiate the fatigue crack [14]. The maximum fatigue strength was obtained at 350°C at Ce containing weld metal, presence of maximum amount of retained austenite content (46.7%).

The fracture surface of welded fatigue test specimen after austempering at 300 and 350°C for 2 h holding time are analyzed by SEM studies and the fractographs are shown in **Figure 14**. In **Figure 14**, the fracture surface reveals ductile fracture with dimple formation also some cleavage fracture which is mostly

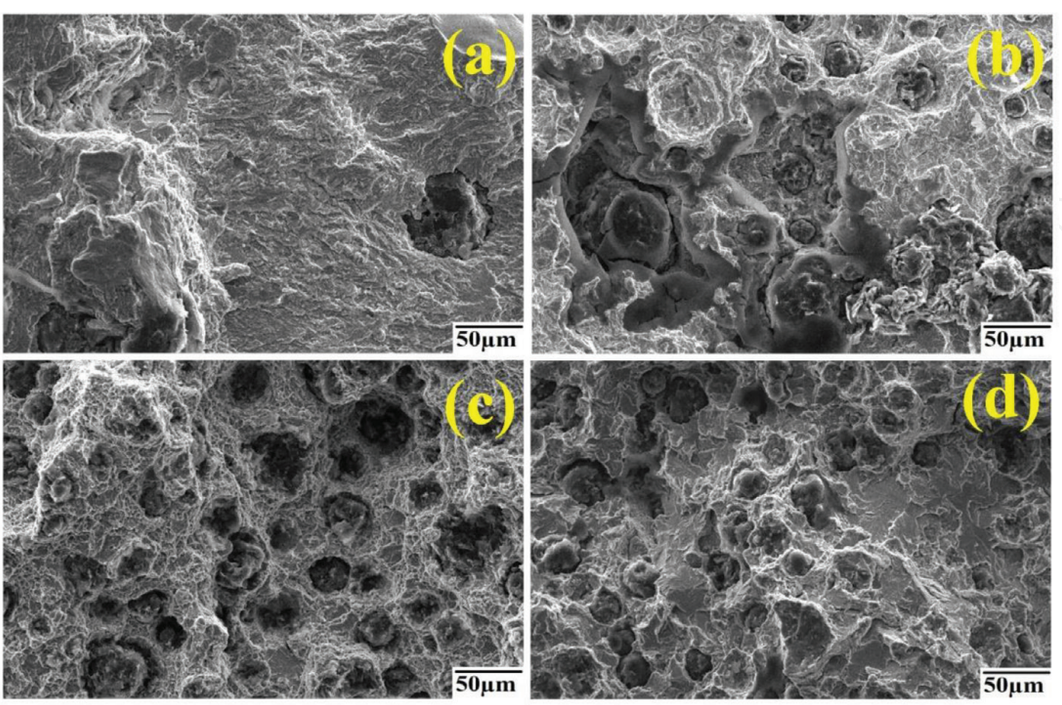

Figure 14.
Fatigue fracture surface austempered ADI weld metals at (a) lower strength and (b) higher strength using Trial 4 electrode and (c) lower strength and (b) higher strength using Trial 7 electrode.

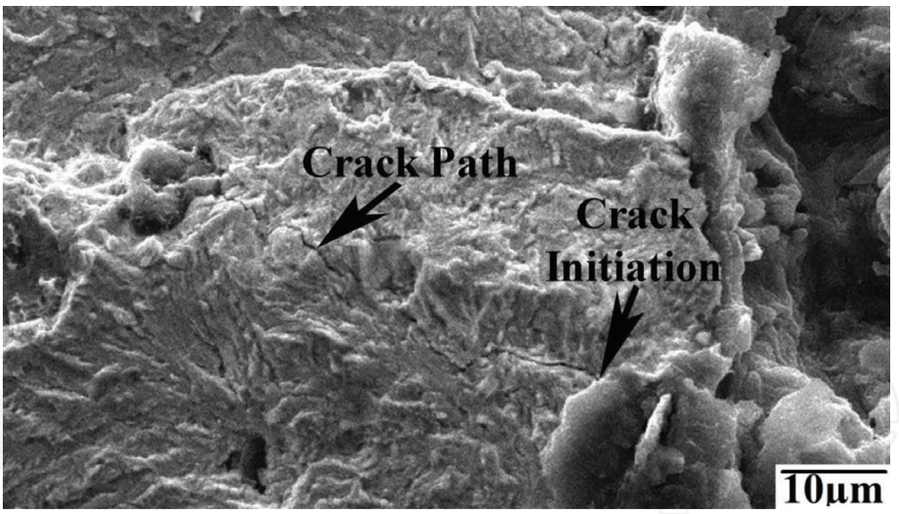

Figure 15.
Fatigue fracture at ADI weld metals indicating the crack initiation and crack propagation path.

occurs in the vicinity of graphite nodules. The combination of ductile striation and cleavage plane whose river patterns go in to tear rivers is named as quasi cleavage [47]. At 300°C (**Figure 14a** and **c**) austempering temperature shoes mixture of dimple and quasi-cleavage fracture, however at 350°C shows (**Figure 14b** and **d**) fully dimple in nature feature is the dominant fracture mechanism to indicate ductile or transgranular in nature. Presence of Ce to refined the fracture surface and shows smaller size dimple in fracture surface and improved the fatigue strength.

The fatigue crack (**Figure 15**) was initiated from the interface between the matrix and graphite nodules and crack path through the least resistance matrix phase due to the week interface bond between graphite and matrix also the lower elastic modulus of graphite. The crack path preferentially intersects with graphite nodules and there is an apparent crack branching mechanism to relate the crack-nodule interactions. This mechanism is responsible for decreasing the fracture energy and reduce the crack propagation rate [48]. **Figure 15** shows, the fatigue crack was initiated comparatively larger size graphite nodules and propagates to the nearest graphite through the matrix surface. The graphite nodules are not perfectly spheroid and the interface between the matrix and graphite are irregulars with multiple sharp corner and high stress concentration to constitute crack that emanate from the graphite nodules [48]. However, the fatigue crack propagation path depends on the next graphite nodules ahead of the crack tip [48] and the crack front connect to the graphite nodules along to the crack path. At higher austempering temperature (350°C), decohesion of nodules and microcracks was observed around the graphite nodules.

It is important to note that several graphite nodules are involved with the growth of crack front, the shape size and distribution of the graphite nodules affects the average growth of crack [49].

Previous investigators [17, 26, 50, 51] states the crack was initiated at the interface between the graphite nodules, and a matrix. However crack also may initiate defects presence in metal such as inclusion, shrinkage and irregular shaped of graphite nodules [52, 53]. The nucleation of the crack grows very rapidly after initiation of crack and decelerates due to the interaction of the matrix structure. The crack is strongly influenced by the microstructure in the crack path region and propagated through discontinuous manner due to the retardation of the matrix grain boundary.

4. Conclusion

Based on the above studies, the following conclusions can be drawn.

1. Both Trial 4 (without Ce) and Trial 7 (with Ce) weld metals are responds in austempering heat treatment at 300 and 350°C for 1.5, 2 and 2.5 h holding time. At 300°C microstructure shows needle shape bainitic ferrite with retained austenite however at 350°C shows feathery shaped bainitic ferrite with retained austenite. Ce content in weld metal to refine the bainitic ferrite and austenite grain size and structures become homogeneous.

2. Volume percentage of retained austenite and its carbon content changed with changing the austempering temperature and holding time. At 300°C shows less amount of retained austenite with higher amount of bainitic ferrite. However at 350°C shows higher amount of retained austenite with comparatively less amount of bainitic ferrite. Retained austenite also varied with varying the austempering holding time at respective temperature and shows maximum retained austenite content at 2 h holding time at each austempering temperature for both the weld metals. However, Ce content in weld metal to enlarge the process windows to delay the stage I reaction and shows more amount of retained austenite at each austempering temperature.

3. The microhardness of weld metal shows lower value at 350°C, presence of higher amount of retained austenite than 300°C austempering temperature. With changing the austempering holding time, the hardness values are changed and show lower hardness value at 2 h holding time with respective austempering temperature. Ce content in weld metal decreased the hardness value and shows at both the temperature, presence of higher amount retained austenite and homogeneous microstructure. Tensile test result shows failure take place from the base metal for both Trial 4 and Trial 7 weld metals at 300 and 350°C for 2 h holding time to indicate the 100% joint efficiency.

4. Charpy impact values are changes with changing the austempering temperature with changing the amount of retained austenite in weld metal. 350°C shows higher impact value for both weld metals presence of higher amount of retained austenite. Ce in weld metal to improve the Charpy impact value as a result of refine the microstructure and increasing the amount of retained austenite. Maximum Charpy impact value shows at Trial 7 weld metal at 350°C austempering conditions.

5. Fatigue strength of both welded joints was improved with improving the austempering temperature. At 350°C feathery shaped bainitic ferrite with higher amount of retained austenite illustrate higher fatigue strength than needle shaped bainitic ferrite with small amount of retained austenite at 300°C. Presence of Ce content in weld metal Trial 7 weld metal shows higher fatigue strength at both austempering temperature due to lower hardness and higher Charpy impact value.

6. Fatigue fracture surface shows at 300°C temperature predominantly mixture with dimple and reverse pattern quasi-cleavage types fracture, however at 350°C shows dimple types fracture to indicates ductile in nature. Ce content

in weld metal to refine the dimple size indicates higher toughness. Crack was initiated in comparatively larger size graphite nodules and propagated through less resistance matrix to the nearest graphite.

IntechOpen

IntechOpen

Author details

Tapan Sarkar
Metallurgical and Material Engineering Department, Welding Technology Centre, Jadavpur University, Kolkata, India

*Address all correspondence to: tapansarkar.met@gmail.com

IntechOpen

© 2019 The Author(s). Licensee IntechOpen. This chapter is distributed under the terms of the Creative Commons Attribution License (http://creativecommons.org/licenses/by/3.0), which permits unrestricted use, distribution, and reproduction in any medium, provided the original work is properly cited. CC BY

References

[1] Panneerselvam S, Putatunda SK, Gundlach R, Boileau J. Influence of intercritical austempering on the microstructure and mechanical properties of austempered ductile cast iron (ADI). Materials Science and Engineering A. 2017;**694**:72-80

[2] Acharya PP, Udupa R, Bhat R. Microstructure and mechanical properties of austempered AISI 9255 high-silicon steel. Materials Science and Technology. 2018;**34**(3):355-365

[3] Bosnjak B, Radulovic B, Pop-Toner K, Asanovic V. Influence of microalloying and heat treatment on the kinetics of bainitic reaction in austempered ductile iron. Journal of Materials Engineering and Performance. 2001;**10**(2):203-211

[4] Lin SC, Lui TS, Chen LH, Song JM. Effect of pearlite on the vibration-fracture behavior of spheroidal graphite cast irons under resonant conditions. Metallurgical and Materials Transactions A. 2002;**33**(8):2623-2634

[5] Lin CK, Lee WJ. Effects of highly stressed volume on fatigue strength of austempered ductile irons. International Journal of Fatigue. 1998;**20**(4):301-307

[6] Chapetti MD. High-cycle fatigue of austempered ductile iron (ADI). International Journal of Fatigue. 2007;**29**(5):860-868

[7] Gundlach RB, Janowak JF. Austempered ductile iron combines strength with toughness and ductility. Metal Progress. 1985;**128**(2):19-26

[8] Ayman H, Elsayed MM, Megahed AA, Sadek KM. Fracture toughness characterization of austempered ductile iron produced using both conventional and two-step austempering processes. Materials and Design. 2009;**30**(6):1866-1877

[9] Panneerselvam S, Martis CJ, Putatunda SK, Boileau JM. Fracture toughness characterization of austempered ductile iron produced using both conventional and two-step austempering processes. Materials Science and Engineering A. 2015;**626**(6):237-246

[10] Putatunda SK. Development of austempered ductile cast iron (ADI) with simultaneous high yield strength and fracture toughness by a novel two-step austempering process. Materials Science and Engineering A. 2001;**315**(1-2):70-80

[11] Kim YJ, Shin H, Park H, Lim JD. Investigation into mechanical properties of austempered ductile cast iron (ADI) in accordance with austempering temperature. Materials Letters. 2008;**62**(3):357-360

[12] Grech M, Young JM. Influence of austempering temperature on the characteristics of austempered ductile iron alloyed with copper and nickel. Transactions of the American Foundrymen's Society. 1990;**98**:345-352

[13] Bartosiewicz L, Krause AR, Alberts FA, Singh I, Putatunda SK. Influence of microstructure on high-cycle fatigue behavior of austempered ductile cast iron. Materials Characterization. 1993;**30**(4):221-234

[14] Puspitasari P, Gapsari F. Fatigue crack growth behavior of nodular cast iron subjected to two-step austempering. Metallurgia. 2018;**57**(4):317-320

[15] Zhang J, Song Q, Zhang N, Lu L, Zhang M, Cui G. Very high cycle fatigue property of high-strength austempered ductile iron at conventional and ultrasonic frequency loading. International Journal of Fatigue. 2015;**70**:235-240

[16] Bahmani M, Elliot R, Varahram N. The relationship between fatigue strength and microstructure in an austempered Cu-Ni-Mn-Mo alloyed ductile iron. Journal of Materials Science. 1997;**32**(20):5383-5388

[17] Shirani M, Härkegård G. Fatigue life distribution and size effect in ductile cast iron for wind turbine components. Engineering Failure Analysis. 2011;**18**(2):1496-1510

[18] Sofue M, Okada S, Sasaki T. High-quality ductile cast iron with improved fatigue strength. In: 82nd Annual Meeting. 1978. pp. 173-182

[19] Diao X, Ning Z, Cao F, Sun J. Effect of CE on graphite nodule count and size distribution in ductile iron. International Journal of Modern Physics B. 2009;**23**(6-7):1853-1860

[20] Choi JO, Kim JY, Choi CO, Kim JK, Rohatgi PK. Effect of rare earth element on microstructure formation and mechanical properties of thin wall ductile iron castings. Materials Science and Engineering A. 2004;**383**(2):323-333

[21] El-Banna EM. Effect of preheat on welding of ductile cast iron. Materials Letters. 1999;**41**(1):20-26

[22] Imasogie BI, Wendt U. Characterization of graphite particle shape in spheroidal graphite iron using a computer-based image analyzer. Journal of Minerals and Materials Characterization and Engineering. 2004;**3**(1):1-12

[23] Sarkar T, Pal TK. Response of austempering heat treatment on microstructure and mechanical property in different zones of as-welded ductile iron (DI). SAE International Journal of Materials and Manufacturing. 2018;**11**(2):151-159

[24] Sarkar T, Pal TK, Pramanick AK. Variation of nano Ce content in austempered ductile iron (adi) weld metal and its effects on microstructure. Transactions of the Indian Institute of Metals. 2018;**71**(10):2375-2385

[25] Zhang J, Li W, Song Q, Zhang N, Lu L. Fatigue of austempered ductile iron with two strength grades in very high cycle regime. Journal of Materials Engineering and Performance. 2016;**25**(3):744-749

[26] Lin CK, Lai PK, Shih TS. Influence of microstructure on the fatigue properties of austempered ductile irons-I. High-cycle fatigue. International Journal of Fatigue. 1996;**18**(5):297-307

[27] Sarkar T, Pramanick AK, Pal TK. Some aspects on the welding characteristics and formation of microstructures in a newly developed coated electrode for austempered ductile iron (ADI). Indian Welding Journal. 2015;**48**(4):44-60

[28] Sarkar T, Pramanick AK, Pal TK, Pramanick AK. Development of a new coated electrode with low nickel content for welding ductile iron and its response to austempering. International Journal of Minerals, Metallurgy, and Materials. 2018;**25**(9):1090-1103

[29] Guide for Welding Iron Castings, ANSI/AWS D11.2-89 (R2006). An American National Standard Institute; 1988. pp. 52-54

[30] Cullity BD. Elements of X-Ray Diffraction. Reading USA:Addison and Wesley Publishing Company Inc; 1978. pp. 32-106

[31] ASTM E23-16b. Standard Test Methods for Notched Bar Impact Testing of Metallic Materials. West Conshohocken, PA: ASTM International; 2016

[32] ASTM E466-15. Standard Practice for Conducting Force Controlled Constant Amplitude Axial Fatigue Tests of Metallic Materials.

West Conshohocken, PA: ASTM International; 2015

[33] Nuri Y, Tetsuro O, Takeshi H, Osamu K. Solidification microstructure of ingots and continuously cast slabs treated with rare earth metal. Transactions of the Iron and Steel Institute of Japan. 1982;**22**:399-407

[34] Xu G, Xiao J. New frontiers in rare earth science and applications. In: Proceedings of the International Conference on Rare Earth Development and Applications. Beijing the People's Republic of China Academic Press; 10-14 September 1985; 1985

[35] Jiang MZ, Yu YC, Li H, Ren X, Wang SB. Effect of rare earth cerium addition on microstructures and mechanical properties of low carbon high manganese steels. High Temperature Materials and Processes. 2017;**36**(2):145-153

[36] Qingxiang Y, Bo L, Jianhua L, Mei Y. Effect of rare earth elements on carbide morphology and phase transformation dynamics of high Ni-Cr alloy cast iron. Journal of Rare Earths. 1998;**16**:36-40

[37] Zhi X, Liu J, Xing J, Shengqiang M. Effect of cerium modification on microstructure and properties of hypereutectic high chromium cast iron. Materials Science and Engineering A. 2014;**603**:98-103

[38] Fernandino DO, Massone JM, Boeri RE. Characterization of the austemperability of partially austenitized ductile iron. Journal of Materials Processing Technology. 2013;**213**(10):1801-1809

[39] Mallia J, Grech M. Effect of silicon content on impact properties of austempered ductile iron. Materials Science and Technology. 1997;**13**(5):408-414

[40] Abioye AA, Atanda PO, Abioye OP, Afolalu SA, Dirisu JF. Microstructural characterization and some mechanical behaviour of low manganese austempered ferritic ductile iron. International Journal of Applied Engineering Research. 2017;**12**(23):13435-13441

[41] Putatunda SK, Jiang HY. A novel processing of austempered ductile cast iron (ADI). Materials Science Forum. 2003;**426**:913-918

[42] Rao PP, Putatunda SK. Dependence of fracture toughness of austempered ductile iron on austempering temperature. Metallurgical and Materials Transactions A. 1998;**29**(12):3005-3016

[43] Wang B, Barber G, Sun X, Shaw M, Seaton P. Characteristics of the transformation of retained austenite in tempered austempered ductile iron. Journal of Materials Engineering and Performance. 2017;**26**(5):2095-2101

[44] Putatunda SK, Martis C. Influence of two-step austempering process on the fracture toughness of a low carbon low alloy (LCLA) steel. Materials Science Forum. 2012;**706**:2259-2264

[45] Batra U, Ray S, Prabhakar SR. Impact properties of copper-alloyed and nickel-copper alloyed ADI. Journal of Materials Engineering and Performance. 2007;**16**(4):485-489

[46] Li XH, Saal P, Gan WM, Hoelzel M, Volk W, Petry W, et al. Strain-induced martensitic transformation kinetic in austempered ductile iron (ADI). Metallurgical and Materials Transactions A. 2018;**49**(1):94-104

[47] Lin CK, Wei JY. High-cycle fatigue of austempered ductile irons in various-sized Y-block castings. Materials Transactions, JIM. 1997;**38**(8):682-691

[48] Bullooch JH. Near threshold fatigue behaviour of flake graphite cast irons microstructures. Theoretical

and Applied Fracture Mechanics. 1995;**24**(1):65-78

[49] Greno GL, Otegui JL, Boeri RE. Mechanisms of fatigue crack growth in austempered ductile iron. International Journal of Fatigue. 1999;**21**(1):35-43

[50] Stokes B, Gao N, Reed PAS. Effects of graphite nodules on crack growth behaviour of austempered ductile iron. Materials Science and Engineering A. 2007;**445**:374-385

[51] Jen KP, Wu J, Kim S. The study of fracture and fatigue behavior of austempered ductile iron. AFS Trans. 1992;**92**:133-164

[52] Lin CK, Fu CS. Low-cycle fatigue of austempered ductile irons in various-sized Y-block castings. Materials Transactions, JIM. 1997;**38**(8):692-700

[53] Lin CK, Chang CW. Influence of heat treatment on fatigue crack growth of austempered ductile iron. Journal of Materials Science. 2002;**37**(4):709-716